Available online at www.sciencedirect.com
SCIENCE DIRECT®
Lithos 74 (2004) 117–130
LITHOS
www.elsevier.com/locate/lithos

Magmatic differentiation examined with a numerical model considering multicomponent thermodynamics and momentum, energy and species transport

Takeshi Kuritani*

The Pheasant Memorial Laboratory for Geochemistry and Cosmochemistry, Institute for Study of the Earth's Interior, Okayama University, Misasa, Tottori 682-0193, Japan

Received 10 June 2003; accepted 9 December 2003

Available online 8 March 2004

Abstract

Magmatic differentiation processes in a cooling magma body were examined using a numerical model considering multicomponent thermodynamics and momentum, energy and species transport. The model accounts for melt transport induced by its density variation, resulting primarily from solid–liquid phase change. The equilibrium mineral assemblages, their mass fractions and their chemical compositions are determined by multicomponent thermodynamic models, and these parameters are linked with the calculations of velocity, pressure, temperature and species fields at each iteration and time step. For simplicity, solid phases are assumed to be stationary, and only olivine and plagioclase that are the earliest crystallization phases in common basaltic magmas are considered as fractionating phases. Application of the model to natural magmatic system shows that crystallization occurs selectively along the chilled boundaries soon after the cooling, and the magma body is separated into high-crystallinity mush zones and mostly crystal-free main magma. Because of the melt exchange between the mush zones and the main magma by compositional convection, the main magma evolves progressively in composition and the spatial chemical heterogeneity is grown with time. The melt segregated from the sidewall mush zone is accumulated below the roof mush zone, forming compositional stratification in the upper part of the main magma. On the other hand, the fractionated melt from the floor mush zone principally mixes with the overlying ambient magma in the middle and lower parts of the main magma body. This study shows that the direct treatment of nonlinear coupling among momentum, energy and species transport provides useful information of the thermal and chemical evolution of magma chambers as a function of time and space.

Keywords: Magmatic differentiation; Numerical simulation; Momentum transport; Multicomponent thermodynamics; Major elements

1. Introduction

Quantitative understanding of the thermal and chemical evolution of a differentiating magma body is one of the main goals of petrology. Since the pioneering studies of Bowen (1928), fractional crystallization has been regarded as one of the most principal magmatic processes, and experimental studies have been made extensively to investigate equilibrium state of magmas as a function of temperature, pressure and bulk magma composition (e.g. Walker et

* Fax: +81-858-43-3450.
E-mail address: kuritani@misasa.okayama-u.ac.jp (T. Kuritani).

0024-4937/$ - see front matter © 2003 Elsevier B.V. All rights reserved.
doi:10.1016/j.lithos.2003.12.007

al., 1979; Rutherford et al., 1985; Thy, 1991; Grove et al., 1992; Toplis and Carroll, 1995). And now, solid–liquid equilibria in multicomponent magmatic system can be predicted reliably by thermodynamic models (e.g. Nielsen, 1988; Ghiorso and Sack, 1995). These models enable to calculate quantitatively differentiation trends of magmas with additional treatment of the solid–liquid separation, such as a perfect fractional crystallization and a boundary layer fractionation (e.g. Nielsen and Delong, 1992). However, such calculations solely consider the mass balance and cannot express the chemical evolution as a function of time.

To simulate the thermal and chemical evolution of magmas as a function of time and space, some studies have combined multicomponent thermodynamic models with the constraint of energy balance between cooling magmas and the surrounding crust, by assuming a local equilibrium (Ariskin et al., 1993; Kuritani, 1999a). Because of a lack of the constraint of momentum balance, however, these models also require the artificial treatment of the relative phase motion between crystals and melt. Magmatic differentiation of natural system proceeds through complex physical processes with nonlinear coupling among the momentum, energy and species transport (Jaupart and Tait, 1995; Spera et al., 1995).

From these reasons, it is necessary to have a model including both multicomponent thermodynamics and conservations of mass momentum, energy and species, for full understandings of magmatic differentiation. This approach is, however, faced with some difficulties. At first, incorporation of multicomponent thermodynamics into the transport model is difficult, because the multicomponent thermodynamic model itself is complex. In addition, many solid phases, including olivine, plagioclase, augite, orthopyroxene, titanomagnetite and apatite, would appear during cooling from the liquidus to the solidus of magmas, and therefore it takes much time to perform computations. Previous studies have, therefore, concentrated solely on the simplified magmatic systems, such as $CaAl_2Si_2O_8$–$CaMgSi_2O_6$ system (Oldenburg and Spera, 1991) and $KAlSi_2O_6$–$CaMgSi_2O_6$ system (Spera et al., 1995). Another difficulty concerns the treatment of motion of solid phases. The transport model considering motions of solid and liquid phases is much more complex than the model solely with liquid phase motion. Although the transport models treating motions of both phases have been developed (e.g. Ni and Incropera, 1995), it is still technically difficult to apply them to magmatic systems. In addition, the model including motion of solid phases requires information of crystal size distributions at a given crystal content. However, the parameters controlling the crystallization kinetics have not adequately been accumulated in multicomponent magmatic systems, which further hinders to apply the transport model including solid phase motion to the natural magmatic system.

In this study, a magmatic differentiation model including multicomponent thermodynamics and conservations of mass momentum, energy and species is developed with some model assumptions, as a necessary first step towards the goal. The model assumes that only olivine and plagioclase are the crystallization phases, by which the difficulty for treating many solid phases is reduced. The region with a solid mass fraction of >60% is not solved using the constraint of thermodynamics. It is clear that the consideration of only these two solid phases is not enough to simulate correctly the differentiation of actual magmas. However, this study focuses much on examining the features of magmatic differentiation using the model including multicomponent thermodynamics and momentum balance. It is further assumed that the solid phases are stationary. Although this is an unrealistic assumption in the actual magmatic system, the model is expected to provide useful qualitative information of the differentiation processes especially for the early stage of the evolution, in which the main part of the magma body is mostly free of crystals. At first, the model descriptions are given for some details. The model is then applied to natural magmatic system, and the thermal and chemical evolution of a cooling magma is examined. Finally, the features of magmatic differentiation in the natural magmatic systems, implied from the results of the simulation, are discussed.

2. The model

Solidification is considered in a two-dimensional, rectangular impermeable cavity of dimensions $X \times Y$ (Fig. 1). A set of continuum conservation equations for solid–liquid phase change system (Bennon and Incropera, 1987a; Prescott and Incropera, 1991) is

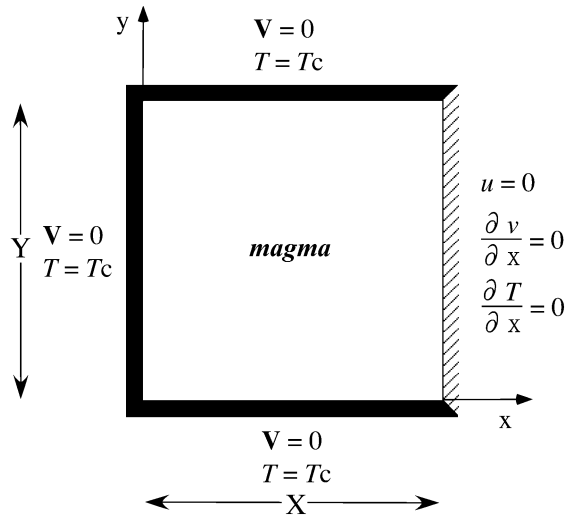

Fig. 1. Domain and boundary conditions for simulation of magmatic differentiation. The roof, floor and left vertical walls are held at T_c, on the other hand, the right vertical boundary is insulated.

applied to basaltic magma system by incorporating multicomponent thermodynamic models. The continuum conservation equations for mass, momentum, energy and species may be expressed as:

continuity

$$\frac{\partial}{\partial t}(\rho) + \nabla \cdot (\rho \mathbf{V}) = 0 \tag{1}$$

x-momentum

$$\frac{\partial}{\partial t}(\rho u) + \nabla \cdot (\rho \mathbf{V} u) = \nabla \cdot \left(\mu_l \frac{\rho}{\rho_l} \nabla u\right) - \frac{\mu_l}{K}\frac{\rho}{\rho_l}(u - u_s) - \frac{\partial p}{\partial x} \tag{2}$$

y-momentum

$$\frac{\partial}{\partial t}(\rho v) + \nabla \cdot (\rho \mathbf{V} v) = \nabla \cdot \left(\mu_l \frac{\rho}{\rho_l} \nabla v\right) - \frac{\mu_l}{K}\frac{\rho}{\rho_l}(v - v_s) - \frac{\partial p}{\partial y} - \rho g \tag{3}$$

energy

$$\frac{\partial}{\partial t}(\rho T) + \nabla \cdot (\rho \mathbf{V} T) = \nabla \cdot (\rho \kappa \nabla T) + \frac{\rho L}{c}\frac{\partial f_s}{\partial t} \tag{4}$$

species for i-th component

$$\frac{\partial}{\partial t}(\rho C_i) + \nabla \cdot (\rho \mathbf{V} C_i) = \nabla \cdot (\rho D_i \nabla C_i) + \nabla \cdot [\rho D_i \nabla (C_{li} - C_i)] - \nabla \cdot [\rho (\mathbf{V} - \mathbf{V}_s)(C_{li} - C_i)] \tag{5}$$

where t is the time, ρ is the density, $\mathbf{V}$ is the velocity vector, u is the x-velocity, v is the y-velocity, μ is the viscosity, K is the permeability, p is the pressure, g is the acceleration due to gravity, T is the temperature, κ is the thermal diffusivity, L is the latent heat of crystallization, c is the specific heat, f is the mass fraction of either solid or liquid phase, C is the composition, D is the mass diffusion coefficient, and subscripts i, l and s denote i-th species component, liquid and solid, respectively. Although Bennon and Incropera (1987a) adopted enthalpy-based energy conservation to consider crystallization at the constant eutectic temperature, this study used the temperature-based energy equation to introduce multicomponent thermodynamic models that include temperature as an explicit parameter. The mixture continuum properties, including density, velocity, thermal diffusivity and chemical diffusivity, are defined as

$$\phi = f_s \phi_s + f_l \phi_l \tag{6}$$

where ϕ is a general field variable (ρ, u, v, C, D). Assumptions in the formulation of Eqs. (1)–(5) are: (i) saturated mixture conditions ($f_s + f_l = 1$); (ii) laminar and Newtonian flow in the liquid phase; (iii) Boussinesq approximation; and (iv) local thermodynamic equilibrium (Bennon and Incropera, 1987a). The species diffusion in the solid phase is also ignored, because it is negligible compared with that of the melt phase. The important assumption of (iv) may be valid in magmatic system, which has been suggested from the studies of Hawaiian lava lakes (Tait and Jaupart, 1996). The multiphase region ($0 < f_l < 1$) is viewed as a porous solid characterized by an isotropic permeability K, and the Kozeny-Carman equation is used

$$K = K_0 \left[\frac{f_l^3}{(1 - f_l)^2}\right] \tag{7}$$

where K_0 is a constant which depends on the specific multiphase region morphology. Note that modeling of the solid–liquid interaction force using this relationship is basically valid only for the laminar flow through a porous medium ($f_l < \sim 0.5$).

The continuum conservation equations are further simplified by assuming the solid phase to be stationary ($\mathbf{V}_s = 0$). This is an unrealistic assumption in the actual magmatic systems, because settling of crystals is one of the most important mechanisms to cause a chemical heterogeneity of magmas. However, this mechanism may be much less important than other mechanisms, such as a convective melt exchange involving mush zones, when the crystallinity of the main part of the magma body is low (e.g. Kuritani, 1999b). On the other hand, processes such as crystal-laden plumes originated from the roof boundary layer and slumping of the sidewall mush zone cannot be reproduced by the current model with the assumption of $\mathbf{V}_s = 0$.

Calculations of phase mass fractions and phase compositions, required to close the system of conservation equations, are performed using multicomponent thermodynamic models. However, many crystal phases would appear during cooling from the liquidus to the solidus temperatures even in basaltic magma system, and it is very difficult to take all the crystal phases into account using thermodynamic models. For simplicity, only olivine and plagioclase, the earliest crystallization phases in common basaltic systems, are considered as solid phases, and thermodynamic calculations are restricted to the regions in which the liquid mass fraction f_l is greater than 0.4. For the regions with $f_l > 0.4$, equilibrium mineral assemblages, their proportions and the interstitial melt composition are calculated using the thermodynamic solution models for olivine of Hirschmann (1991), for plagioclase of Elkins and Grove (1990) and for silicate melt of Ghiorso and Sack (1995) at a given local magma composition and temperature at each iteration and time step. These solution models are internally consistent with the thermodynamic database of Berman (1988) (Ghiorso and Sack, 1995). The density of the interstitial melt for the buoyancy term in Eq. (3) and the latent heat of crystallization are obtained by Lange and Carmichael (1990) and Berman (1988), respectively. In the regions with $f_l < 0.4$, on the other hand, thermodynamic calculations are not performed due to the presence of "incompatible" major elements, such as TiO_2, K_2O and P_2O_5. From this reason, the interstitial melt composition cannot be calculated, and therefore, the motion of the melt phase is not considered (i.e. $\mathbf{V}_l = 0$) in this region. This assumption does not significantly affect the results, because the motion of the melt phase would be fairly low due to high crystallinity ($f_s > 0.6$). The liquid mass fraction is assumed to decrease linearly with temperature to zero at the solidus temperature T_s. The latent heat of crystallization is assumed to be a constant value, L_m, in this region. Because of these treatments, in addition to the assumption of no motion of solid phases, the application of the present model may be limited to the early stage of the evolution of basaltic magma system, in which olivine and plagioclase are the dominant crystallization phases and the main part of the magma body is mostly free of crystals.

Multicomponent magmas in this model consist of 12 species: SiO_2, TiO_2, Al_2O_3, Fe_2O_3, FeO, MnO, MgO, CaO, Na_2O, K_2O, P_2O_5 and H_2O. Because this study solely considers olivine (Mg_2SiO_4–Fe_2SiO_4) and plagioclase ($CaAl_2Si_2O_8$–$NaAlSi_3O_8$), the species can be reduced to seven components: SiO_2, Al_2O_3, FeO, MgO, CaO, Na_2O and MO, where MO includes TiO_2, Fe_2O_3, MnO, K_2O, P_2O_5 and H_2O. Due to the constraint of $\Sigma C_i = 1$, six components are independent in the above seven species, and thus six equations are required for the species conservation (Eq. (5)). Dissolved water may be locally saturated during crystallization of hydrous magmas. The water solubility as a function of pressure, temperature and melt composition is obtained from the model of Moore et al. (1998), which constrains the thermodynamic calculations. The relative motion between vapor and melt phases is not considered. Variation of the equilibrium ferric–ferrous ratio in silicate melt during magmatic evolution, CaO and MnO in olivine, and K_2O in plagioclase are ignored.

Each of the conservation equations (Eqs. (1)–(5)) can be cast into the general form

$$\frac{\partial}{\partial t}(\rho\phi) + \nabla \cdot (\rho \mathbf{V}\phi) = \nabla \cdot (\Gamma \nabla \phi) + S_\phi \qquad (8)$$

where ϕ is a general continuum dependent variable, Γ is diffusion coefficient and S_ϕ represents source term. Discretization of these equations was performed

according to the method described in Bennon and Incropera (1988), and they were solved with an elliptic control-volume-based finite difference scheme (Patanker, 1981).

Before applying the model to multicomponent magma system, the code of the model was verified. The first test case was a simple one-dimensional pure diffusion problem. The verification of the model for this problem was easily done, by comparing calculated diffusion profiles with analytic solutions. The model was also applied to diffusion-dominated binary solidification problem for $NH_4Cl–H_2O$ system, simulated previously by Bennon and Incropera (1988). The calculated temperature, liquid composition and positions of solidus and liquidus fronts were in good agreement with the results shown in Bennon and Incropera (1988). A two-dimensional solidification with convection problem was then carried out for $NH_4Cl–H_2O$ system, using the same parameters used in Bennon and Incropera (1987b). The verification of the model for this problem was performed by comparing the calculated velocity, temperature and compositional fields with those shown in Bennon and Incropera (1987b). In these simulations, the enthalpy-based energy conservation equation was used, instead of Eq. (4).

3. Results and discussion

3.1. Application of the model to natural magmatic system

As an application of the model to multicomponent magmatic system, calculations were performed for alkali basalt (Kutsugata lava) erupted from Rishiri Volcano, Japan (Kuritani, 1998). The composition of the least differentiated samples of the lava (Table 1) was used as an initial magma composition for the simulation. Calculated phase diagram for this composition at the pressure condition of 2 kbars is shown in Fig. 2a. In actual system, other solid phases than olivine and plagioclase, such as augite and hornblende, would appear at temperatures higher than 900 °C.

The conservation equations were solved for the cavity with a size 500 × 500 m ($X \times Y$), using 30 × 30 grid cells. Initially, the cavity was filled with a homogeneous magma of the composition shown in Table 1. Initial magma temperature was 1117 °C, which is the liquidus of the magma at the pressure condition of 2 kbars (Fig. 2a). Solidification was induced by keeping the roof, floor and left sidewall at T_c (600 °C), whereas the right vertical boundary is insulated. This corresponds to simulate the cooling of the left half of the two-dimensional magma body with a size $2X \times Y$. The boundary conditions for temperature and velocity are shown in Fig. 1. The values for the physical parameters adopted here are summarized in Table 2. Other parameters, such as L (latent heat of crystallization in the region $f_l > 0.4$) and ρ_l (density of melt), are calculated for individual grid cells at each iteration and time step, as described above. Note that the value of K_0 has not yet been well determined and may vary by several orders of magnitude, depending on the crystal size and crystal morphologies. The chemical diffusion coefficient in melt D_{li} must be defined carefully in multicomponent system. However, the diffusion coefficient of 1×10^{-11} m^2 s^{-1} (e.g. Hofmann, 1980) is assumed for all the species, because the diffusive transport is negligible compared with the advective transport, and therefore the calculated results are not affected at all.

Table 1
Initial magma composition for the simulation

Component	(wt.%)
SiO_2	51.4
TiO_2	1.37
Al_2O_3	18.0
Fe_2O_3	8.59
MnO	0.14
MgO	5.79
CaO	9.72
Na_2O	4.15
K_2O	0.58
P_2O_5	0.28
H_2O	4.00

The composition is recalculated for the total Fe as Fe_2O_3. Ferric–ferrous ratio in the initial magma is calculated by the model of Sack et al. (1980) with oxygen fugucity of NNO buffer. Water content of 4 wt.% at 2 kbars is from Kuritani (1999c).

The simulation was performed using a personal computer with 1.7 GHz CPU, and it took about 2 months to complete computations for the magmatic evolution in 100 years. In the simulation, time step of the calculation was 0.1 year. To avoid false convergence, the number of iterations was taken for at least 300. Iterations within each time step were terminated

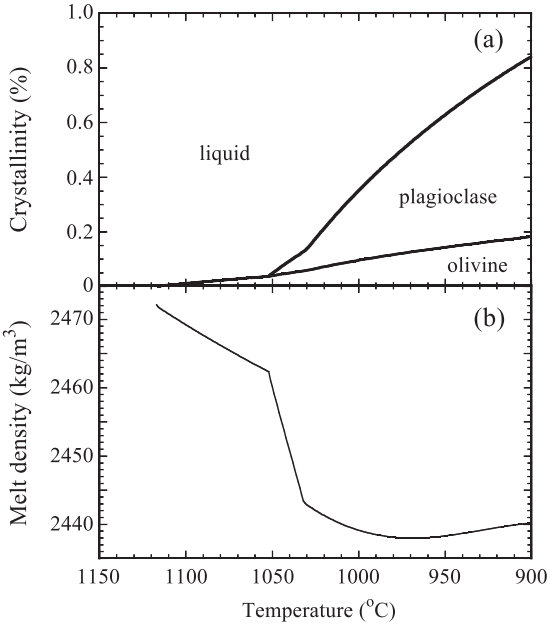

Fig. 2. Calculated phase diagram (a) and calculated density of melt phase (b) as a function of temperature, for the least differentiated compositions of the Kutsugata-lava magma (Kuritani, 1998) at the pressure condition of 2 kbars.

when the local changes in the phase mass fractions, temperature and species compositions (seven species) were all less than 1×10^{-5} relative to the absolute values from one iteration to the next. But the local changes of such parameters were mostly less than 1×10^{-6} after the 300 iterations, and therefore, the numbers of iterations were commonly 300. The differences between the initial homogeneous magma composition (Table 1) and the bulk compositions of the whole magma chamber at the end of the calculation ($t = 100$ years) were at most 0.003 % (relative to the absolute values) for all the elements. This observation confirms that the convergences of the calculations were satisfactory.

3.2. Limitations on the accuracy of the numerical results

Before presenting the results of the numerical calculations, limitations on the accuracy of the numerical results must be noted. As is described above, some critical simplifications are made in the model, such as no motion of solid phase and ignorance of other crystallization phases than olivine and plagioclase, in order to apply the model to multicomponent magmatic systems. In addition to these simplifications, there are also some severe limitations upon simulating magmatic differentiation processes using the current numerical model.

Christenson et al. (1989) compared the results of laboratory experiments with those of numerical calculation based on the model of Bennon and Incropera (1987a,b) for solidification of a binary $NH_4Cl–H_2O$ solution. Although some important features of the solidification process were satisfactory predicted by the numerical calculations, quantitative agreement was not fully obtained between the numerical results and the experimental observations, resulting partly from the adoption of the Kozeny-Carman equation for the whole crystallization interval and uncertainty of the parameter K_0. These problems are common in the numerical calculations of this study.

The size of grid cells of 30×30 are undoubtedly not adequate to resolve actual magmatic differentia-

Table 2
Parameters used in the numerical calculation

Parameters	Values	Remarks
T_i = initial magma temperature (°C)	1117	
T_c = cooling temperature (°C)	600	
T_s = solidus temperature (°C)	650	assumed
P = pressure condition of magma body (bars)	2000	Kuritani (1998)
g = acceleration due to gravity (m s^{-2})	9.8	
κ_s = thermal diffusivity of solid (m^2 s^{-1})	8×10^{-7}	
κ_l = thermal diffusivity of liquid (m^2 s^{-1})	8×10^{-7}	
c_s = specific heat of solid (J kg^{-1} K^{-1})	1.3×10^3	
c_l = specific heat of liquid (J kg^{-1} K^{-1})	1.3×10^3	
μ = viscosity of magma (kg m^{-1} s^{-1})	8.5	calculated after Shaw (1972)
D_{si} = chemical diffusivity in solid (m^2 s^{-1})	0	
D_{li} = chemical diffusivity in liquid (m^2 s^{-1})	1×10^{-11}	see text
L_m = latent heat of crystallization, $f_l < 0.4$ (J kg^{-1})	3×10^5	
K_0 = permeability coefficient (m^2)	5×10^{-10}	Oldenburg and Spera (1991)

tion processes occurred in cooling magma bodies. For example, the width of the melt channels (formed by compositional convection) in the mush zones along the chamber walls has probably a length scale of less than a meter (e.g. Jellinek and Kerr, 1999), much smaller than one grid spacing of ~17 m of this simulation. In addition, magmatic processes simulated with the two-dimensional grid could differ from those calculated with the three-dimensional grid. For example, "axisymmetric" plumes reproduced in the two-dimensional model correspond to sheet-like plumes in three dimensions, although compositional plumes in real (three-dimensional) magma chambers are axisymmetric. Jellinek et al. (1999) actually showed by laboratory experiments that the convective mixing of sheet-like plumes is more efficient than the convective mixing of axisymmetric plumes, due to the greater interaction of the sheets. Although these problems may be overcome by performing the simulation with grid spacing of, e.g. $500 \times 500 \times 500$, such calculations need to be carried out using an extremely high-performance supercomputer, and therefore, could be a future work.

From these limitations, the current numerical model is expected not to make reliable *quantitative* predictions of the thermal and chemical evolution of cooling magmas. In spite of this, however, the model including momentum balance would provide useful *qualitative* information of magmatic differentiation processes, which are not obtained from models considering solely energy and/or mass balances.

3.3. Overview of magmatic differentiation

Fig. 3 shows the evolution of temperature (left side) and the bulk SiO_2 content with fluid velocity field (right side) of the cooling magma, for different time steps, 3, 10, 30 and 100 years. The vertical profiles of some parameters across the magma body at $X = 250$ m are also shown in Fig. 4. Soon after the cooling, crystallization occurs along the chilled boundaries. In the Kutsugata magma system, the density of the melt phase decreases and then increases with decreasing the temperature from the liquidus (Fig. 2b). The inflection of the density variation at 1050 °C results from the appearance of plagioclase, and the inflection at 1032 °C reflects that the water is saturated in the melt at temperatures lower than 1032 °C. The density minimum appears at about 970 °C, at which solid mass fraction is about 0.5. Because of this effect, solutally driven flows (compositional convection) are induced along the all boundaries, by which the bulk compositions of the boundary layers are progressively depleted in SiO_2 (Fig. 3) and K_2O (Fig. 4b), and enriched in MgO (Fig. 4a) with time. In the floor and sidewall mush zones, the convective melt exchange is caused by the density contrast between the interstitial melt and the mostly crystal-free main magma. On the other hand, compositional convection along the roof boundary is induced by the density difference of the interstitial melt *within* the roof mush zone. Along the vertical wall of the magma chamber, the rise of the buoyant differentiated melt is dominated within the mush zone, and the melt flows laterally to mix with the main magma below the roof boundary layer. This type of melt flow along the sidewall boundary was observed in laboratory experiments by Bédard et al. (1992). In the floor boundary layer, the melt exchange occurs between the mush zone and the overlying ambient main magma, as observed in analogue experiments using aqueous solutions (e.g. Tait et al., 1992).

Simultaneously with the compositional changes in the boundary layers, differentiation of the main magma ($f_s \sim 0$) proceeds by mixing of the fractionated melt from the mush zones, and the main magma becomes enriched in incompatible elements and depleted in compatible elements. These features are similar to those observed in igneous complexes (e.g. Shirley, 1987; McBirney, 1995) and analogue experiments using aqueous solutions (Chen, 1995). The melt flow of the main magma near the floor boundary layer forms some convecting cells (Fig. 3), and the lower and middle parts of the main magma (at the levels of 100–300 m) are thermally and chemically homogeneous. On the other hand, compositional and thermal gradient is established in the upper part of the main magma (300–400 m). Around the contact between the main magma and the floor mush zone, the focused regions dominated by upflow of melt ("chimney"; e.g. Tait and Jaupart, 1992) are relatively cool and those dominated by downflow have higher temperature (e.g. $t = 100$ years in Fig. 3). Note that the size of the convecting cells and the width of the chimney of the numerical results probably reflect the artificial

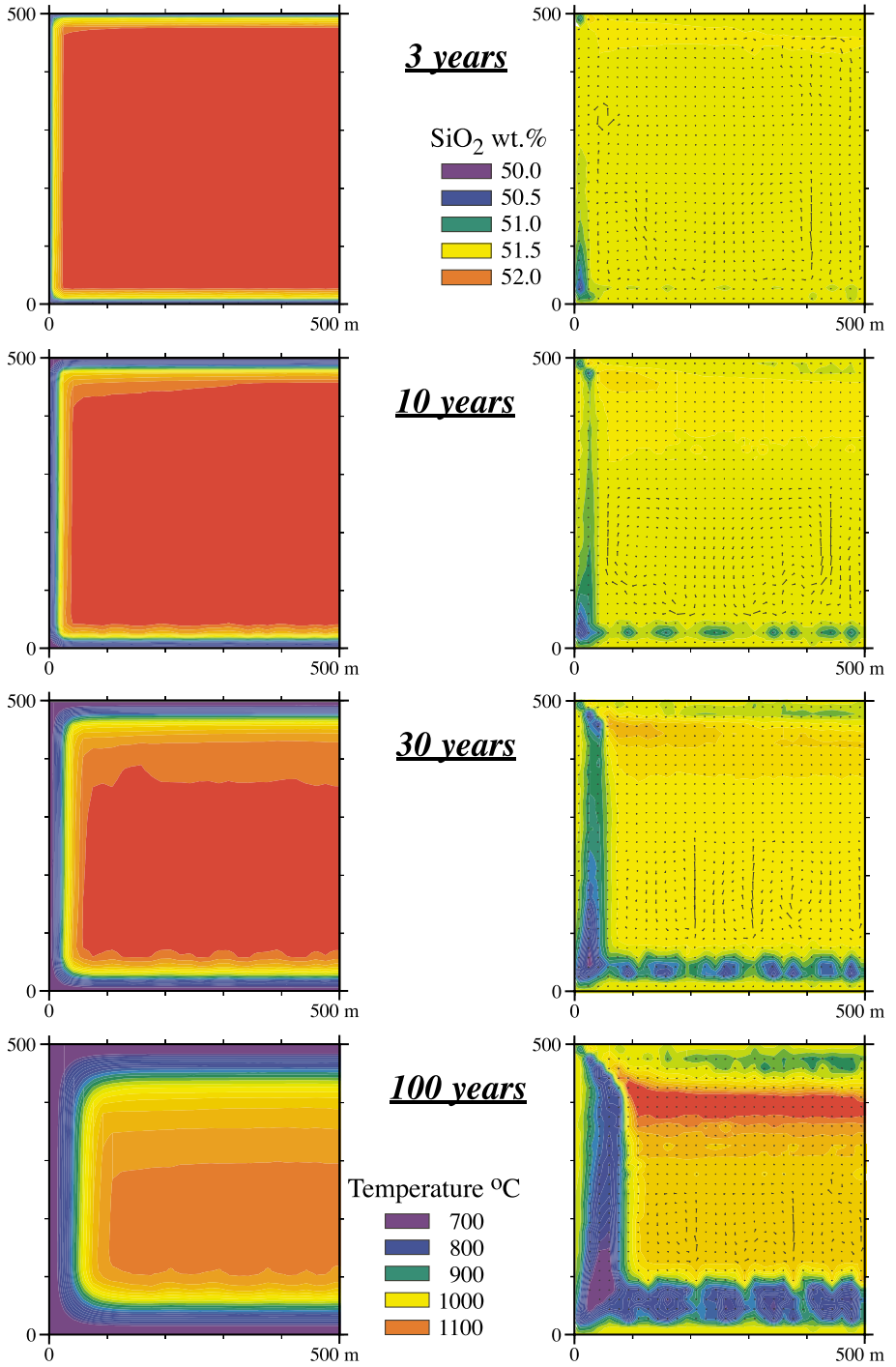

Fig. 3. Isotherms (left side) and isopleths of bulk SiO_2 content, along with velocity fields (right side) at 3, 10, 30, and 100 years. The maximum velocity is 2.9×10^{-5} m/s at 3 years, 3.3×10^{-5} m/s at 10 years, 4.2×10^{-5} m/s at 30 years and 3.2×10^{-5} m/s at 100 years (right side).

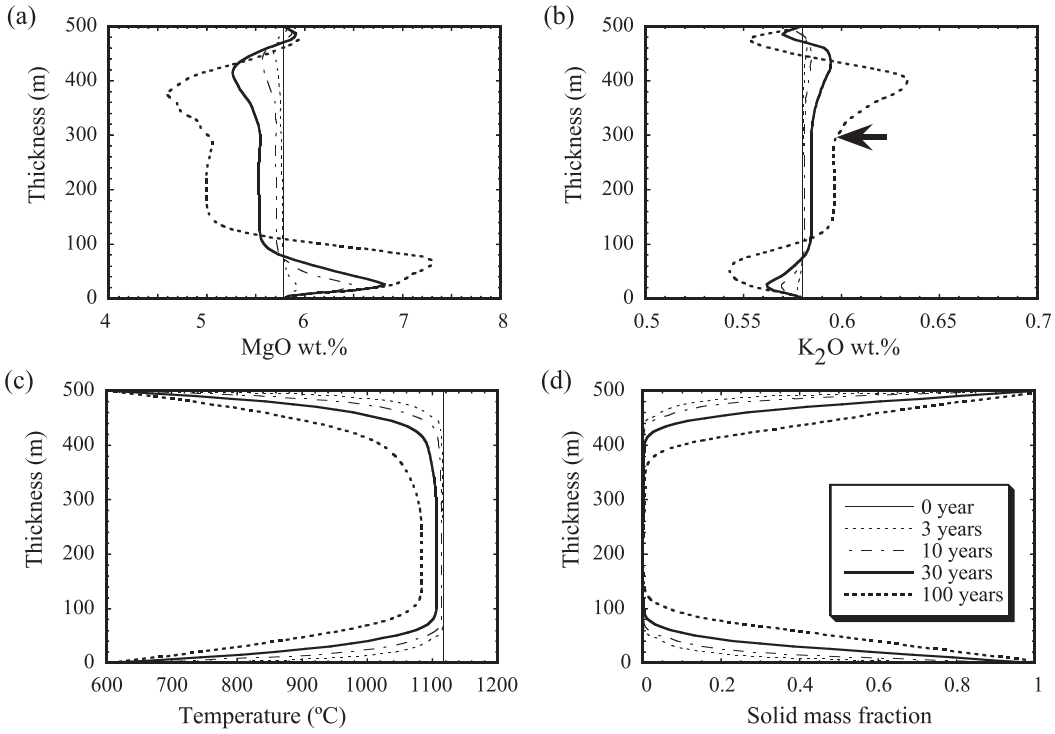

Fig. 4. Profiles of (a) MgO content, (b) K_2O content, (c) temperature, and (d) solid mass fraction, for the vertical section at $X = 250$ m. Arrow in (b) indicates the boundary which divides the contribution of the floor mush zone and that of the sidewall mush zone to the chemical evolution of the main magma. See text for details.

effect of the wide grid spacing (30×30) used in this simulation, and thus these length scales have no quantitative significance.

The thermal gradient near the floor is steeper than that of the roof (Fig. 4c). This reflects the heating of the floor mush zone by introduction of hot melt from the main magma by compositional convection. Contrary to the asymmetric temperature profile, the variation of the solid mass fraction (f_s) is mostly symmetric for the roof and floor boundary layers (Fig. 4d). In the upper part of the main magma, crystallization is suppressed by the effect of liquidus depression, by enrichment of rejected components including Na_2O, K_2O and H_2O, despite that the temperature is lower than other part of the main magma. Although the growth of the floor boundary layer is suppressed by influx of the hot melt from the main magma as described above, the growth of the roof boundary layer is also suppressed by the effect of liquidus depression.

3.4. Formation of chemical heterogeneity in the main magma

Fig. 5 shows the variations of the maximum, average and minimum SiO_2 content of the mostly crystal-free main magma (defined here as $f_s < 0.002$) with time. The range between the maximum and minimum contents is, therefore, the compositional variation established in the main magma. Such time-dependent spatial variation of chemical compositions cannot be predicted reliably unless models include the momentum transport. The average SiO_2 content increases progressively with time, resulting from the melt exchange between the main magma and mush zones, as is discussed above. The trend of the average SiO_2 content is much closer to that of the minimum content, which reflects that the less differentiated homogeneous magma present in the middle and lower parts is dominated in the total volume of the main magma. Soon after the cooling, relatively large com-

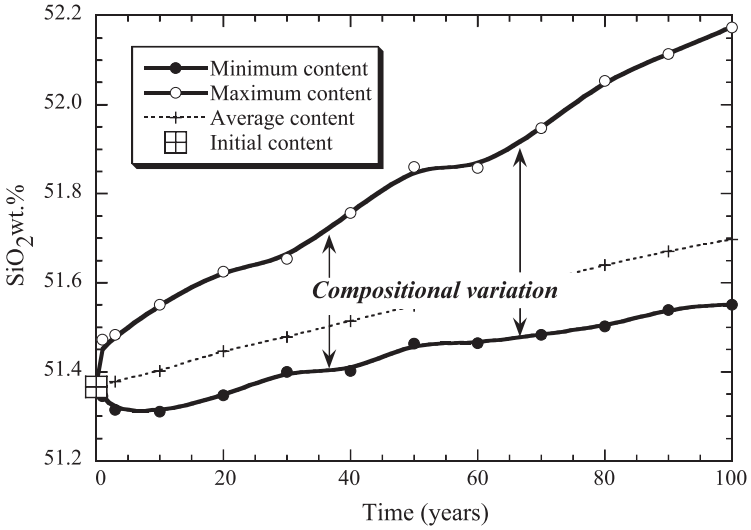

Fig. 5. The variation of the maximum, average and minimum SiO_2 content of the main magma with time, from 0 to 100 years. The region that falls within the range between the maximum and minimum trends is the compositional variation established in the main magma.

positional variation is formed and the variation continues to become enlarged with shifting to the higher SiO_2 content. The gradient of the maximum SiO_2 content is steeper than that of the average and minimum contents, which results from the imperfect mixing of the fractionated melt from the mush zones with the main magma.

3.5. Compositional trends of the main magma

Fig. 6 compares the compositions of the spatially heterogeneous main magma at 50 years with those of the perfect fractional crystallization trend obtained purely by thermodynamic calculations (solely with mass conservation). The inflection of the perfect fractionation trend at about 51.8 wt.% SiO_2 reflects the appearance of plagioclase, in addition to olivine. The simulated compositions have higher MgO content and lower CaO content than the perfect fractionation trend at a given SiO_2 content. This results from that the perfect fractionation trend is produced by separation of liquidus phase (high-Mg # olivine); on the other hand, the compositional variation of the magma obtained by the simulation is formed by fractionation of crystal phases (low-Mg # olivine and plagioclase) that appear at temperatures lower than the liquidus. The latter fractionation mechanism is called "in situ fractionation" or "boundary layer fractionation", and formations of fractionation trends with such features have been predicted by previous studies (Langmuir, 1989; Nielsen and Delong, 1992; Kuritani, 1999a,b).

3.6. Implications for magmatic processes

It is shown above that the model considering mass momentum, energy and species conservations provides useful information on magmatic differentiation, especially the time-dependent spatial variation of the physical variables. This model also gives a chance to examine the features of magmatic processes that cannot be investigated by the previous approaches, such as petrological observation, experimental studies using analogue materials and theoretical studies without constraints of either multicomponent thermodynamics or momentum balance. In this section, the role of the floor and sidewall mush zones on the chemical evolution of the main magma is briefly examined.

The aspect ratio of magma bodies is one of the most important parameters controlling the features of magmatic differentiation (e.g. de Silva and Wolff, 1995), although this parameter is commonly inaccessible from erupted materials. The fundamental physical principles are the same in the floor and sidewall boundary layers; however, the directions of the density gradients are different with respect to gravity (Jaupart and Tait, 1995). The relative contributions

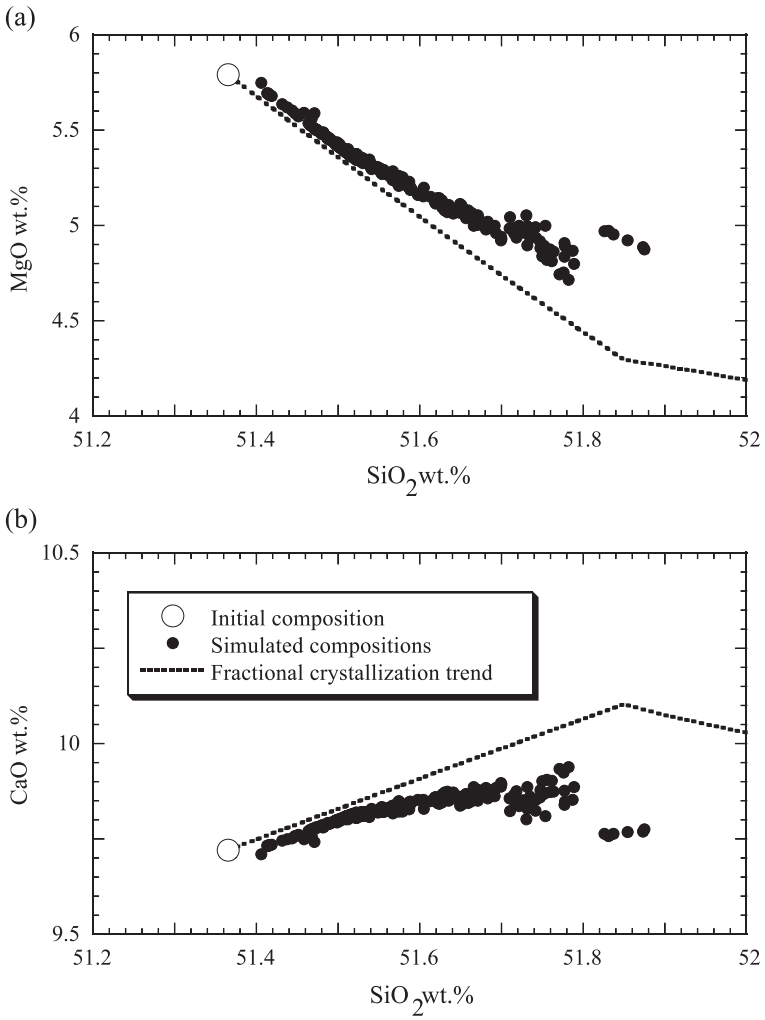

Fig. 6. The compositions of the heterogeneous main magma of the model calculation at 50 years and the perfect fractional crystallization trend, compared in (a) $MgO-SiO_2$ and (b) $CaO-SiO_2$ diagrams. Initial magma composition for the two-dimensional simulation and for the calculation of the perfect fractional crystallization trend is shown with open circle.

of the floor and sidewall mush zones to the chemical evolution of the overall main magma can roughly be evaluated using bulk compositions of the mush zones and the initial composition. At 100 years, the volume of the floor and sidewall mush zones are similar (Fig. 3), and the calculated bulk K_2O content of the floor and sidewall mush zones is 0.549 and 0.536 wt.%, respectively. Because the initial K_2O content is 0.58 wt.%, the "degree of depletion" of the both mush zones can be calculated easily, and thus the relative contributions of the floor and sidewall mush zones is obtained to be approximately 2:3. From this result, it is suggested that the vertical mush zone plays significantly more important role on the compositional evolution of the main magma than the floor mush zone, at a given length scale of the boundaries (here, $X = Y = 500$ m).

There is a strong compositional gradient in the upper part of the main magma (Figs. 3 and 4a,b). The fractionated melt segregated from the sidewall mush zone moves upward along the wall without extensive interactions with the main magma, and then spread laterally below the roof mush zone. Although the fractionated melt from the floor mush zone seems

to mix principally with the overlying ambient magma, the melt may partly reach below the roof boundary layer and may contribute significantly to the formation of the compositional stratification. The relative contribution of the sidewall and floor mush zones to the formation of the chemical heterogeneity of the main magma can also be roughly evaluated. At 100 years, the lateral compositional variation is insignificant (Fig. 3) except for the regions around the sidewall mush zone, and the vertical chemical heterogeneity of the main magma can be approximated to be a one-dimensional, such as those shown in Fig. 4a and b. In the K_2O diagram, for example, the area surrounded by the profile with ≥ 0.58 wt.% at 100 years and the line at 0.58 wt.% ($100\ m < Y < 450\ m$) shows the integration of chemical differentiation of the main magma from 0 to 100 years. Given that the upflow of the fractionated melt from the sidewall did not mix with the middle and lower parts of the main magma, the boundary which divides the contribution from the floor much zone and that of the sidewall mush zone can be delineated (shown with arrow in Fig. 4b), using the ratio of 2:3 determined above. The position of the boundary mostly coincides with the boundary between the heterogeneous upper main magma and the homogeneous middle and lower main magma. This suggests that the fractionated melt extracted from the floor mush zone mixes extensively with the overlying ambient main magma, and does not significantly contribute to the formation of the compositional stratification in the upper part of the main magma. Although the prediction of the extensive mixing of the melt from the basal mush zone with the main magma might partly result from the "two-dimensional effect" discussed above, it is suggested that the melt derived from the sidewall mush zone plays dominant role on the formation of the chemical heterogeneity in the main magma.

Above discussions reconfirms that the sidewall boundary layer has a great significance for the formation of spatial chemical diversity of the main magma, i.e. the compositional variation of eruptible magmas (e.g. McBirney, 1980; de Silva and Wolff, 1995). When the sidewall mush zone is much less important, such as in a sill-like magma body, spatial compositional variation of the main magma is limited and the time for the main magma to evolve to a certain SiO_2 content is much delayed. From the magma chamber in which the sidewall boundary layers are important, relatively large volumes of thermally and chemically zoned magmas are expected to be erupted. Quantitative investigations of the relationship between the chamber geometry (including the size of magma bodies) and the formation of the spatial chemical heterogeneity of the main eruptible magmas could be one of the most attractive future targets using the model presented in this study.

4. Conclusion

Differentiation processes of a multicomponent magma in a cooling magma body were examined using a model considering multicomponent thermodynamics and momentum, energy and species transport. The direct treatment of nonlinear coupling among momentum, energy and species transport provides useful information on the time-dependent spatial variation of the physical variables in the evolving magma chamber. Such information is not obtained from models solely with energy and/or mass balances. Although the present model has some limitations, such as no motion of solid phases, this study is a very important step forward in quantitative understandings of the thermal and chemical evolution of a cooling magma body, which has been one of the main goals of petrology.

Acknowledgements

I thank Kazuhito Ozawa, Hiroko Nagahara and Hikaru Iwamori for constructive discussion and encouragement throughout this study. Constructive reviews and comments by R.C. Kerr and A.A. Ariskin significantly improved the paper. I also thank S. Foley for editorial handlings. I acknowledge E. Nakamura, N. Matsumoto, R. Tanaka and all the other members of the Pheasant Memorial Laboratory at ISEI for encouragement and useful comments. This work was supported by the program for the Center of Excellence for the 21st Century in Japan.

References

Ariskin, A.A., Frenkel, M.Y., Barmina, G.S., Nielsen, R.L., 1993. COMAGMAT: a Fortran program to model magma differentiation processes. Computers & Geosciences 19, 1155–1170.

Bédard, J.H., Kerr, R.C., Hallworth, M.A., 1992. Porous sidewall and sloping floor crystallization experiments using a reactive mush: implications for the self-channelization of residual melts in cumulates. Earth and Planetary Science Letters 111, 319–329.

Bennon, W.D., Incropera, F.P., 1987a. A continuum model for momentum, heat and species transport in binary solid–liquid phase change systems: I. Model formulation. International Journal of Heat and Mass Transfer 30, 2161–2170.

Bennon, W.D., Incropera, F.P., 1987b. A continuum model for momentum, heat and species transport in binary solid–liquid phase change systems: II. Application to solidification in a rectangular cavity. International Journal of Heat and Mass Transfer 30, 2171–2187.

Bennon, W.D., Incropera, F.P., 1988. Numerical analysis of binary solid–liquid phase change using a continuum model. Numerical Heat Transfer 13, 277–296.

Berman, R.G., 1988. Internally-consistent thermodynamic data for minerals in the system Na_2O–K_2O–CaO–MgO–FeO–Fe_2O_3–Al_2O_3–SiO_2–TiO_2–H_2O–CO_2. Journal of Petrology 29, 445–522.

Bowen, N.L., 1928. The Evolution of the Igneous Rocks. Dover, New York. 332 pp.

Chen, C.F., 1995. Experimental study of convection in a mushy layer during directional solidification. Journal of Fluid Mechanics 293, 81–98.

Christenson, M.S., Bennon, W.D., Incropera, F.P., 1989. Solidification of an aqueous ammonium chloride solution in a rectangular cavity: II. Comparison of predicted and measured results. International Journal of Heat and Mass Transfer 32, 69–79.

de Silva, S.L., Wolff, J.A., 1995. Zoned magma chambers: the influence of magma chamber geometry on sidewall convective fractionation. Journal of Volcanology and Geothermal Research 65, 111–118.

Elkins, L.T., Grove, T.L., 1990. Ternary feldspar experiments and thermodynamic models. American Mineralogist 75, 544–559.

Ghiorso, M.S., Sack, R.O., 1995. Chemical mass transfer in magmatic processes: IV. A revised and internally consistent thermodynamic model for the interpolation and extrapolation of liquid–solid equilibria in magmatic systems at elevated temperatures and pressures. Contributions to Mineralogy and Petrology 119, 197–212.

Grove, T.L., Kinzler, R.J., Bryan, W.B., 1992. Fractionation of Mid-Ocean Ridge Basalt (MORB). Geophysical Monograph 71, 281–310.

Hirschmann, M., 1991. Thermodynamics of multicomponent olivines and the solution properties of $(Ni,Mg,Fe)_2SiO_4$ and $(Ca,Mg,Fe)_2SiO_4$ olivines. American Mineralogist 76, 1232–1248.

Hofmann, A.W., 1980. Diffusion in natural silicate melts: a critical review. In: Hargraves, R.B. (Ed.), Physics of Magmatic Processes. Princeton Univ. Press, Princeton, pp. 385–417.

Jaupart, C., Tait, S.R., 1995. Dynamics of differentiation in magma reservoirs. Journal of Geophysical Research 100, 17615–17636.

Jellinek, A.M., Kerr, R.C., 1999. Mixing and compositional stratification produced by natural convection: 2. Applications to the differentiation of basaltic and silicic magma chambers and komatiite lava flows. Journal of Geophysical Research 104, 7203–7218.

Jellinek, A.M., Kerr, R.C., Griffiths, R.W., 1999. Mixing and compositional stratification produced by natural convection: 1. Experiments and their application to Earth's core and mantle. Journal of Geophysical Research 104, 7183–7201.

Kuritani, T., 1998. Boundary layer crystallization in a basaltic magma chamber: evidence from Rishiri Volcano, northern Japan. Journal of Petrology 39, 1619–1640.

Kuritani, T., 1999a. Thermal and compositional evolution of a cooling magma chamber by boundary layer fractionation: model and its application for primary magma estimation. Geophysical Research Letters 26, 2029–2032.

Kuritani, T., 1999b. Boundary layer fractionation constrained by differential information from the Kutsugata lava flow, Rishiri Volcano, Japan. Journal of Geophysical Research 104, 29401–29417.

Kuritani, T., 1999c. Phenocryst crystallization during ascent of alkali basalt magma at Rishiri Volcano, northern Japan. Journal of Volcanology and Geothermal Research 88, 77–97.

Lange, R.L., Carmichael, I.S.E., 1990. Thermodynamic properties of silicate liquids with emphasis on density, thermal expansion and compressibility. In: Nicholls, J., Russell, J.K. (Eds.), Modern Methods of Igneous Petrology: Understanding Magmatic Processes. Mineralogical Society of America, Washington, DC, pp. 25–64.

Langmuir, C.H., 1989. Geochemical consequences of in situ crystallization. Nature 340, 199–205.

McBirney, A.R., 1980. Mixing and unmixing of magmas. Journal of Volcanology and Geothermal Research 7, 357–371.

McBirney, A.R., 1995. Mechanisms of differentiation in the Skaergaard intrusion. Journal of the Geological Society (London) 152, 421–435.

Moore, G., Vennemann, T., Carmichael, I.S.E., 1998. An empirical model for the solubility of H_2O in magmas to 3 kilobars. American Mineralogist 83, 36–42.

Ni, J., Incropera, F.P., 1995. Extension of the continuum model for transport phenomena occurring during metal alloy solidification: I. The conservation equations. International Journal of Heat and Mass Transfer 38, 1271–1284.

Nielsen, R.L., 1988. A model for the simulation of combined major and trace element liquid lines of descent. Geochimica et Cosmochimica Acta 52, 27–38.

Nielsen, R.L., Delong, S.E., 1992. A numerical approach to boundary layer fractionation: application to differentiation in natural magma systems. Contributions to Mineralogy and Petrology 110, 355–369.

Oldenburg, C.M., Spera, F.J., 1991. Numerical modeling of solidification and convection in a viscous pure binary eutectic system. International Journal of Heat and Mass Transfer 34, 2107–2121.

Patanker, S.V., 1981. A calculation procedure for two-dimensional elliptic situations. Numerical Heat Transfer 4, 409–425.

Prescott, P.J., Incropera, F.P., 1991. Modeling of dendritic solidification systems: reassessment of the continuum momentum equation. International Journal of Heat and Mass Transfer 34, 2351–2359.

Rutherford, M.J., Sigurdsson, H., Carey, S., Davis, A., 1985. The May 18, 1980, eruption of Mount St. Helens: 1. Melt composition and experimental phase equilibria. Journal of Geophysical Research 90, 2929–2947.

Sack, R.O., Carmichael, I.S.E., Rivers, M., Ghiorso, M.S., 1980. Ferric–ferrous equilibria in natural silicate liquids at 1 bar. Contributions to Mineralogy and Petrology 75, 369–376.

Shaw, H.R., 1972. Viscosities of magmatic silicate liquids: an empirical method of prediction. American Journal of Science 272, 870–893.

Shirley, D.N., 1987. Differentiation and compaction in the Palisades Sill, New Jersey. Journal of Petrology 28, 835–865.

Spera, F.J., Oldenburg, C.M., Christensen, C., Todesco, M., 1995. Simulations of convection with crystallization in the system $KAlSi_2O_6$–$CaMgSi_2O_6$: implications for compositionally zoned magma bodies. American Mineralogist 80, 1188–1207.

Tait, S.R., Jaupart, C., 1992. Compositional convection in a reactive crystalline mush and melt differentiation. Journal of Geophysical Research 97, 6735–6756.

Tait, S.R., Jaupart, C., 1996. The production of chemically stratified and adcumulate plutonic igneous rocks. Mineralogical Magazine 60, 99–114.

Tait, S.R., Jahrling, K., Jaupart, C., 1992. The planform of compositional convection and chimney formation in a mushy layer. Nature 359, 406–408.

Thy, P., 1991. High and low pressure phase equilibria of a mildly alkalic lava from the 1965 Surtsey eruption: experimental results. Lithos 26, 223–243.

Toplis, M.J., Carroll, M.R., 1995. An experimental study of the influence of oxygen fugacity on Fe–Ti oxide stability, phase relations, and mineral-melt equilibria in ferro-basaltic systems. Journal of Petrology 36, 1137–1170.

Walker, D., Shibata, T., Delong, S.E., 1979. Abyssal tholeiites from the Oceanographer Fracture Zone: II. Phase equilibria and mixing. Contributions to Mineralogy and Petrology 70, 111–125.